BCREC2021_1

by Leny Yuliati

Submission date: 27-Jul-2022 03:55PM (UTC+0800)
Submission ID: 1875756998
File name: erature_on_the_Photocatalytic_Activity_of_Zn2Ti3O8_Materials.pdf (853.14K)
Word count: 5192
Character count: 26833

Available online at BCREC website: https://bcrec.id

Bulletin of Chemical Reaction Engineering & Catalysis, 16 (1) 2021, 196-204

Research Article

Effect of Calcination Temperature on the Photocatalytic Activity of $Zn_2Ti_3O_8$ Materials for Phenol Photodegradation

Krisfian Tata Aneka Priyangga[1], Yehezkiel Steven Kurniawan[1], Leny Yuliati[1,2,*)]

[1]Ma Chung Research Center for Photosynthetic Pigments, Universitas Ma Chung, Malang 65151, East Java, Indonesia.
[2]Department of Chemistry, Faculty of Science and Technology, Universitas Ma Chung, Malang 65151, East Java, Indonesia.

Received: 8th February 2021; Revised: 24th March 2021; Accepted: 24th March 2021
Available online: 25th March 2021; Published regularly: March 2021

Abstract

Zinc titanate ($Zn_2Ti_3O_8$) is a bimetal oxide material that is especially attractive as a photocatalyst. In the preparation of the $Zn_2Ti_3O_8$, the calcination temperature is a crucial parameter. Hence, in the present work, we aimed to synthesize the $Zn_2Ti_3O_8$ materials from zinc(II) nitrate and titanium(IV) isopropoxide as precursors by using a sol-gel method and followed by calcination at 700, 900, and 1100 °C to give ZT-700, ZT-900, and ZT-100 materials, respectively. The ZT materials were characterized using Fourier transform infrared (FTIR), diffuse reflectance ultraviolet-visible (DR UV-vis), and fluorescence spectroscopies. It was confirmed that the ZT materials contained O–Ti–O, Zn–O–Ti, Zn–O, Ti–O–Ti, and Ti–O functional groups as shown from their FTIR spectra. Similar fluorescence properties were only observed on the ZT-700 and ZT-900. From the bandgap energy analysis, ZT-700 and ZT-900 contained spinel and cubic $Zn_2Ti_3O_8$ (spl-$Zn_2Ti_3O_8$ and c-$Zn_2Ti_3O_8$) crystal phases), while ZT-1100 contained c-Zn_2TiO_4 and TiO_2 rutile crystal phases. The kinetic analysis of photocatalytic phenol degradation showed that both ZT-700 and ZT-900 materials exhibited high photocatalytic activity with the reaction rate constants of 0.0353 and 0.0355 h^{-1}, respectively. These values were higher than that of the ZT-1100 (0.0206 h^{-1}). This study demonstrated that calcination at 700 and 900 °C resulted in the formation of the spl-$Zn_2Ti_3O_8$ and c-$Zn_2Ti_3O_8$ phases, which were effective as the photocatalyst, but the formation of c-Zn_2TiO_4 and rutile TiO_2 at calcination of 1100 °C deteriorated the photocatalytic activity.

Keywords: Bimetal oxide; Calcination Temperature; Photocatalyst; Sol-gel; $Zn_2Ti_3O_8$

How to Cite: K.T.A. Priyangga, Y.S. Kurniawan, L. Yuliati (2021). Effect of Calcination Temperature on the Photocatalytic Activity of $Zn_2Ti_3O_8$ Materials for Phenol Photodegradation. *Bulletin of Chemical Reaction Engineering & Catalysis*, 16(1), 196-204 (doi:10.9767/bcrec.16.1.10322.196-204)

Permalink/DOI: https://doi.org/10.9767/bcrec.16.1.10322.196-204

1. Introduction

Phenol is recognized as one organic pollutant that existed in wastewater. Photocatalytic degradation of phenols has been studied by various heterogeneous catalysts, in which titanium dioxide (TiO_2) was mainly explored as the photocatalyst [1–3]. In order to increase the performance of the TiO_2, modifications have been made by creating bimetallic oxides, which are attractive due to their unique properties. Combining two metal oxides could give better properties, which lead to a better photocatalytic activity, such as in the case of zirconium

* Corresponding Author.
Email: leny.yuliati@machung.ac.id (L. Yuliati);
Telp: +62-341-550171, Fax: +62-341-550-175

titanates [4] and zinc titanates [5–9]. Particular attention is made to the zinc titanates ($Zn_xTi_yO_z$, ZT)-based materials, which have been reported as good photocatalysts for either water splitting or photocatalytic degradation of aqueous organic pollutants [5–9]. As an example, when the $Zn_2Ti_3O_8$ was combined with TiO_2 in a thin film for photocatalytic hydrogen evolution, it was found that the material owing to the $Zn_2Ti_3O_8$ phase yielded a remarkable photocatalytic enhancement [5]. On the other hand, the $Zn_2Ti_3O_8$/carbon nitride-zinc oxide materials gave a good photocatalytic activity for the degradation of methylene blue, in which the photocatalytic activity corresponded to the amount of $Zn_2Ti_3O_8$ in the composite material [6]. While the application of zinc titanates seems to be promising, one shall be careful in preparing the material due to the possible formation of different crystallographic phases.

Zinc titanates as semiconductor materials can exist in three different crystallographic phases including $ZnTiO_3$ (cubic, c, and hexagonal, h), Zn_2TiO_4 (cubic, c), and $Zn_2Ti_3O_8$ (spinel, spl, and cubic, c) [10–14]. They were usually prepared by controlling the stoichiometric ratio of Zn^{2+} and Ti^{4+} precursors. In addition to the stoichiometric ratio, selecting the correct temperature during the synthesis would be very important since the stability of the $Zn_2Ti_3O_8$ is strongly affected by temperature and the synthesis method. The stability of the c-$Zn_2Ti_3O_8$ was studied and it was reported that it could be stable up to a temperature of 800 °C [10]. The c-$Zn_2Ti_3O_8$ was reported to form at the low temperature of 500 °C when using zinc chloride ($ZnCl_2$) and titanium chloride ($TiCl_3$) as the precursors and synthesized by a simple precipitation method followed by calcination [15]. However, they reported that the $Zn_2Ti_3O_8$ was transformed to $ZnTiO_3$ when the calcination temperature was increased to 600 °C. Another group reported that calcining zinc oxide (ZnO) and titanium dioxide (TiO_2) with the mol ratio of 2:3 at 750 °C was able to obtain the $Zn_2Ti_3O_8$ phase [16]. Accordingly, the Zn:Ti mol ratio of 2:3 was used in the present work to obtain the $Zn_2Ti_3O_8$ phase.

Since the synthesis temperatures could determine the obtained zinc titanate phase, it is very important to study the effect of calcination temperature on the properties and photocatalytic activity of the zinc titanates. To date, a comprehensive study about the calcination temperature effect on the formation of the $Zn_2Ti_3O_8$, when the Zn:Ti mol ratio is fixed to 2:3 has not been addressed yet. Therefore, in the present work, we conducted the study and examined the photocatalytic activity of the formed $Zn_2Ti_3O_8$ for photocatalytic degradation of phenol. The $Zn_2Ti_3O_8$ material was synthesized using a sol-gel method from the reaction between titanium(IV) isopropoxide and zinc(II) nitrate under alkaline condition followed by calcination at 700, 900, and 1100 °C to give ZT-700, ZT-900, and ZT-1100 materials. The photocatalytic activity of the synthesized materials was studied for the degradation of phenol under ultraviolet (UV) irradiation and the kinetics of photocatalytic phenol degradation was investigated to determine the reaction rate constant.

2. Materials and Methods

2.1 Materials of Research

The used materials in this work were zinc nitrate hexahydrate ($Zn(NO_3)_2{\cdot}6H_2O$, CAS No. 10196-18-6, 98%, Sigma-Aldrich), titanium(IV) isopropoxide (TTIP, $Ti(OC_3H_7)_4$, CAS No. 13463-67-7, 97%, Merck), sodium hydroxide (NaOH, CAS No. 1310-73-2, > 99.9%, Merck), ethanol (C_2H_5OH, CAS No. 64-17-5, > 99.9%, Merck), phenol (C_6H_5OH, CAS No. 108-95-2, 99%, Merck), and acetonitrile (CH_3CN, CAS No. 75-05-8, ≥ 99.93%, Merck).

2.2 Procedures

2.2.1 Synthesis of ZT materials

Zinc nitrate hexahydrate (2.92 g, 0.010 mol) was dissolved in ethanol (10 mL) in a beaker glass to produce solution A, while TTIP (4.27 g, 0.015 mol, 1.5 equivalent) was dissolved in ethanol (10 mL) in another beaker glass to produce solution B. Solution A was poured into the solution B and then NaOH 1.0 M solution (2 mL) was added dropwise into the mixture. The mixture was kept stirred for 1 hour to homogenize the mixture. Afterward, the mixture was dried at 60 °C for 24 hours to evaporate the solvent and allow the sol-gel formation. The formed sol-gel was ground into a powder and calcined at a different temperature of 700, 900, or 1100 °C. The calcination process was conducted with a temperature increase of 700 °C h^{-1} to reach the desired calcination temperature and then the samples were calcined at the certain temperature for 6 hours. The prepared ZT materials at different calcination temperatures of 700, 900, and 1100 °C were abbreviated as ZT-700, ZT-900, and ZT-1100, respectively.

2.2.2 Characterization of ZT materials

The ZT materials were characterized using a Fourier transform infrared (FTIR, JASCO 6800) spectroscopy attached with an attenuated total reflectance (ATR) Pro One accessory (Single-Reflection ATR). The measurement was carried out in the wavenumber range of 4000–400 cm^{-1} to identify the functional groups present in each sample. The diffuse reflectance ultraviolet-visible (DR UV-vis) spectrum of each sample was collected on a UV-vis spectrophotometer (JASCO V-760) using an integrating sphere, ISV-922/ISN-923/ISN-901i accessory, in which the measurement was made in the range of 200–800 nm. The emission and excitation fluorescence spectra of each sample were measured using a fluorescence spectrophotometer (JASCO FP-8500) on an FDA-808 cell holder for the solid powder sample. The fluorescence emission was recorded at $\lambda_{excitation}$ of 274 nm, while the fluorescence excitation was recorded at $\lambda_{emission}$ of 302 nm.

2.2.3 Photocatalytic test of ZT materials

Each of ZT-700, ZT-900, or ZT-1100 as the photocatalyst material (50 mg) was added into 50 $mg.L^{-1}$ of aqueous phenol solution (50 mL). The mixture was stirred under a dark condition for 2 hours at room temperature. The mixture was then illuminated under a UV lamp (UVLS-28 EL Series, 365 nm) for 1, 3, 6, and 24 hours. After the illumination, the sample was filtered and then the phenol concentration in the filtrate was analyzed by high-performance liquid chromatography (HPLC, Shimadzu LC-20 AT) with a photodiode array (PDA) SPD-M20 A detector at 272 nm. The C18 column and acetonitrile were used as the stationary and mobile phases, respectively, and the flow rate was set to 0.8 $mL.min^{-1}$ at 40 °C. The schematic experimental setup for the evaluation of photocatalytic activity is shown in Figure 1. The phenol concentration was measured using a standard calibration curve method and the degradation percentage of phenol was calculated from the ratio of remaining phenol concentration after reaction (C_t) to the one before the reaction (C_0) using Equation (1).

$$Phenol\ degradation\,(\%) = \frac{C_t}{C_0} \times 100\% \quad (1)$$

The kinetic photocatalytic degradation of phenol over the ZT materials was further investigated using the first-order reaction model, as generally occurred in the case of photocatalytic degradation reaction [2] and shown in equation (2). The reaction rate constant (k) was obtained from the gradient of the linear plot between $-\ln(C_t/C_0)$ and reaction time (t).

$$-\ln\left(\frac{C_t}{C_0}\right) = kt \quad (2)$$

2

3. Results and Discussion

3.1 Characterizations of ZT Materials

The ZT materials synthesized at three different calcination temperatures, *i.e.* 700, 900, and 1100 °C, were characterized by using an FTIR spectrometer to identify the functional

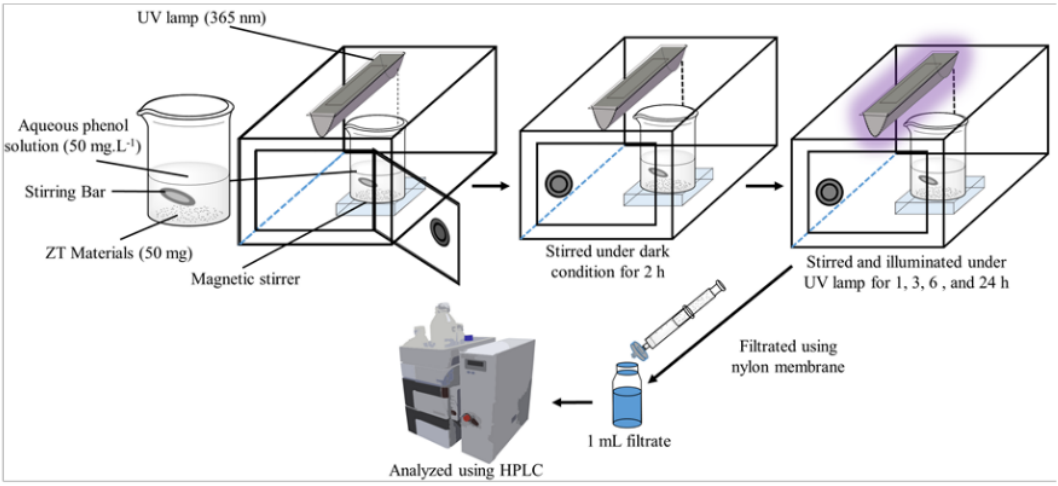

Figure 1. Schematic experimental setup for the evaluation of photocatalytic activity of ZT materials.

groups from the vibrational modes present in these materials. The FTIR spectra of ZT-700, ZT-900, and ZT-1100 are shown in Figure 2. Figure 2(a) shows that increasing the calcination temperature from 700 to 1100 °C resulted in the disappearance of the −OH functional groups (3400 cm^{-1}), which were originated from the adsorbed water molecules [16] on the ZT surface. On the other hand, all composites showed some weak absorption signals in the fingerprint region of 418 cm^{-1} as well as in the range of 545–549, 639–642, 696–708, and 837–990 cm^{-1} (see Figure 2(b)). The sharp band at 418 cm^{-1} could be assigned to the Ti−O bending vibration in $[TiO_6]^{2-}$ octahedral in ZT materials [7]. This was supported by the absorption signals present in a region of 900 cm^{-1} as well as the peaks observed in the range of 639–642 cm^{-1}, which corresponded to the O−Ti−O stretching vibration of $[TiO_6]^{2-}$ octahedral in ZT materials [17]. The characteristic of ZT materials was also shown by a Zn−O−Ti vibration, which was observed as a shoulder band at the region of 696–708 cm^{-1} [18]. On the other hand, the shoulder bands in the range of 545–549 and 501–504 cm^{-1} were also observed due to the presence of $[ZnO_4]^{2-}$ structure in the ZT materials [19,20]. Additionally, a strong signal at 873 cm^{-1} was observed on ZT-700, which was related to the vibration of Ti−O stretching involving non-bridging oxygen atoms. As the calcination temperature increased, the intensity of this peak on the ZT-900 and ZT-1100 was decreased and shifted to the higher wavenumber, indicating a crystal phase transformation of $Zn_2Ti_3O_8$ at a higher temperature, which affected the nature of this vibrational mode.

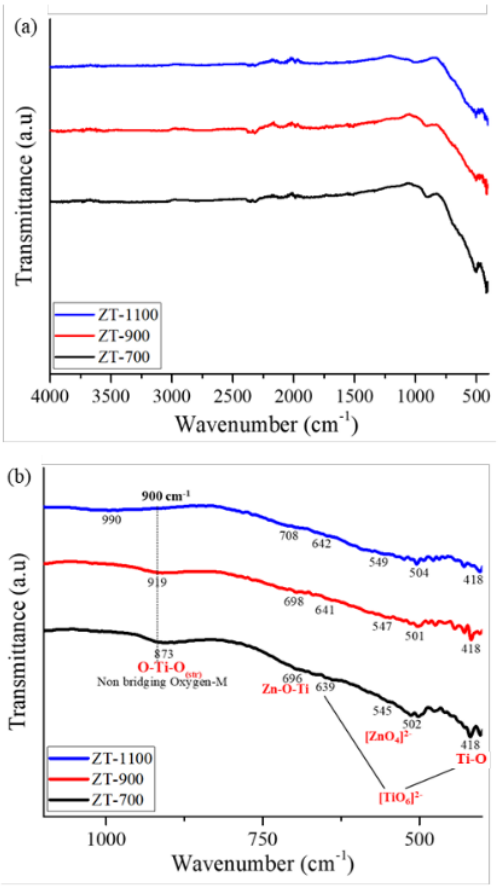

Figure 2. FTIR spectra of ZT materials shown as (a) full spectra at 400–4000 cm^{-1} and (b) magnified spectra at 400–1100 cm^{-1}.

The DR UV-vis spectra of the ZT materials synthesized at three different calcination temperatures were also recorded to study the optical properties and calculate the bandgap energy of these semiconductor materials. The DR UV-vis spectra were plotted in Kubelka-Munk function versus wavelength as shown in Figure 3. All the ZT materials obtained at different calcination temperatures showed significant absorptions in the UV region, but not in the visible region, which was in accordance with the white color of these materials as shown in Figure 4.

The ZT-700 showed absorption peaks at 214, 254, and 286 nm. When the calcination temperature was increased to 900 °C, the absorption peaks were observed at 214, 254, and 339 nm. While the absorption peaks at 214 and 254 nm were not changed as compared to those

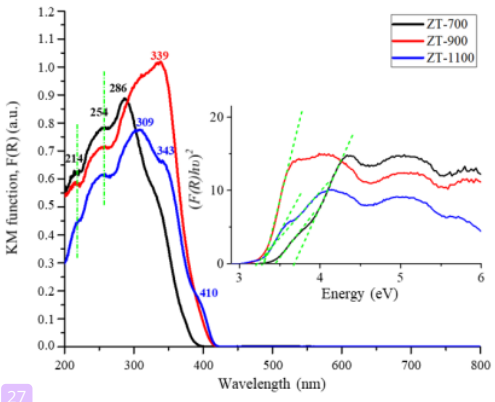

Figure 3. DR-UV Vis spectra of ZT materials and the Tauc plots (inset) for bandgap energy determination.

of the ZT-700, the broadening and peak shifting was observed from 286 to 339 nm. This change indicated that some amounts of $Zn_2Ti_3O_8$ were transformed to $ZnTiO_3$, which was in agreement with the previous report [7]. For the ZT-1100, the band at 214 nm nearly vanished and the band at 254 nm was significantly decreased. Meanwhile, the absorption at 286 nm was also decreased and a new peak was observed at a higher wavelength of 309 nm. In addition, new absorption band and shoulder peak were also observed at 343 and 410 nm, respectively. All these changes could be ascribed to a major transformation of $Zn_2Ti_3O_8$ into the other crystal phases (*i.e.* Zn_2TiO_4 and rutile TiO_2) due to the high temperature [21,22].

The determination of bandgap energy values is important for photocatalyst application since it gives information on the minimum energy required to excite the electrons from the valence band to the conduction band of semiconductor material. The direct bandgap energy values of all the $Zn_2Ti_3O_8$ materials were calculated using the Tauc method as shown in equation (3), where α, h, Eg, and υ are the absorption coefficient of the materials, Planck constant (6.636×10^{-34} J.s), bandgap energy (eV), and light frequency (Hz), respectively. The α value can be replaced by the value of Kubelka-Munk function, F(R) [23] as also performed in this work.

$$(\alpha h\upsilon)^2 = A(Eg - h\upsilon) \quad (3)$$

The bandgap energy values can be then determined by extrapolating the linear plot between the $(\alpha h\upsilon)^2$ versus $(h\upsilon)$ to the x-axis. The Tauc plots for the bandgap energy measurement of the $Zn_2Ti_3O_8$ samples are also shown as the inset in Figure 3. The bandgap energy values of each ZT material and other reported values for zinc titanates and rutile TiO_2 are summarized in Table 1. According to the reported literature, the bandgap value of c-$Zn_2Ti_3O_8$ would be in the range of 3.20–3.50 eV [5,6], for spl-$Zn_2Ti_3O_8$ in the range of 3.56 eV or higher [8,24], for c-Zn_2TiO_4 would be in the range of 3.22–3.45 eV [25], while for rutile TiO_2 in the range of 3.00–3.20 eV [26,27]. Therefore, it can be proposed here that the ZT-700 would

ZT-700 **ZT-900** **ZT-1100**

Figure 4. Photographs of the ZT materials as white solid powder.

Table 1. Assignment of bandgap energy values of the ZT and TiO_2 materials.

Sample	Bandgap energy (eV)	Assignment	Reference
ZT-700	3.64, 3.42	spl-$Zn_2Ti_3O_8$ and c-$Zn_2Ti_3O_8$	This work
ZT-900	3.32	c-$Zn_2Ti_3O_8$	This work
ZT-1100	3.28, 3.19	c-Zn_2TiO_4 and rutile TiO_2	This work
Zinc titanate	3.20–3.50	c-$Zn_2Ti_3O_8$	[5,6]
Zinc titanate	≥ 3.56	spl-$Zn_2Ti_3O_8$	[8,24]
Zinc titanate	3.22–3.45	c-$ZnTiO_4$	[25]
TiO_2	3.00–3.20	rutile TiO_2	[26,27]

have spl-$Zn_2Ti_3O_8$ and c-$Zn_2Ti_3O_8$, the ZT-900 would have c-$Zn_2Ti_3O_8$ as a main phase, while the ZT-1100 would have c-Zn_2TiO_4 and rutile TiO_2. The different formed phases were possibly observed as the $Zn_2Ti_3O_8$ could be decomposed to $ZnTiO_4$ and rutile TiO_2 at a high temperature of 1100 °C [21,22].

The fluorescence spectra of ZT-700, ZT-900, and ZT-1100 materials are shown in Figure 5. As depicted in Figure 5(a), all the ZT materials exhibited a strong excitation peak at 274 nm when monitored at an emission wavelength of 302 nm. While a similar level of excitation intensity could be observed in the ZT-700 and ZT-900, a higher intensity was observed in the ZT-1100. Figure 5(b) shows the emission spectra of ZT-700, ZT-900, and ZT-1100 when measured using 274 nm as the excitation wavelength. All the samples gave the same main emission peak at 302 nm. A similar trend was observed here that the ZT-700 and ZT-900 gave similar emission intensity, while the ZT-1100 gave higher emission intensity than the other ZT materials. The higher emission intensity could be related to the high electron-hole recombination, which could play important role in photocatalytic reactions. In addition to the emission peak at 302 nm, some emission peaks were also observed in the range of 350–700 nm. It was clear that the ZT-700 and ZT-900 gave similar emission peaks in this region, showing the similar characteristics between ZT-700 and ZT-900, which could be ascribed to the presence of the $Zn_2Ti_3O_8$ phase in these two materials. In contrast, the ZT-1100 gave a different shape of emission spectrum, suggesting that a different phase existed on the ZT-1100. As described above, the $Zn_2Ti_3O_8$ phase could be transformed into Zn_2TiO_4 and TiO_2 rutile phase in the ZT-1100, which in turn led to exhibit different emission spectrum.

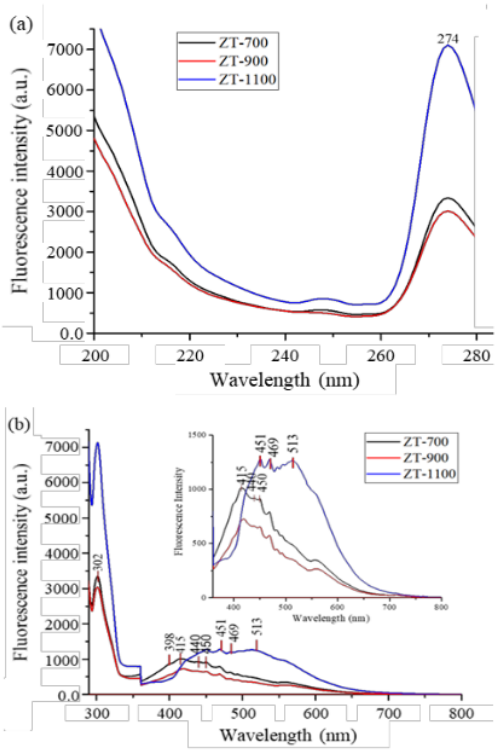

Figure 5. (a) Excitation and (b) emission spectra of ZT materials monitored at an emission wavelength of 302 nm and an excitation wavelength of 274 nm, respectively. Inset shows the magnified emission spectra at 360–800 nm.

3.2 Photocatalytic Activity of ZT Materials

The performance of ZT-700, ZT-900, and ZT-1100 materials as photocatalysts was evaluated for the photocatalytic degradation of phenol.

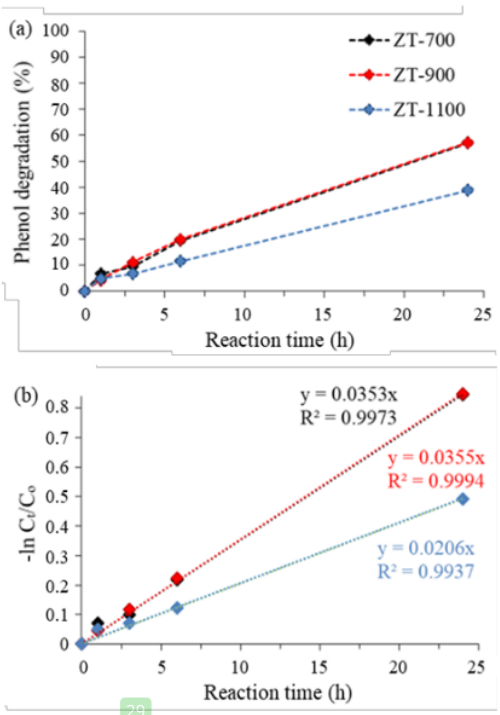

Figure 6. Photocatalytic degradation of phenol under UV light irradiation on ZT materials shown as plots of (a) phenol degradation (%) versus reaction time and (b) −ln (C_t/C_0) versus reaction time.

Figure 6(a) shows the plot between phenol degradation percentage versus the reaction time. It could be observed that the ZT-700 and the ZT-900 photocatalysts showed similar photocatalytic activity to each other, which was higher than that of the ZT-1100. After 24 hours-reaction, the ZT-700 and the ZT-900 gave 57% phenol degradation, while the ZT-1100 only gave 39%. This different result would be strongly affected by the different phases that existed in the ZT materials. The ZT-700 and the ZT-900 showed a similar level of high activity as they have the $Zn_2Ti_3O_8$ phase. In contrast, the ZT-1100 gave a lower photocatalytic activity due to the absence of the $Zn_2Ti_3O_8$ phase. Therefore, it was demonstrated that the calcination temperature determined the type of ZT phase formed in the synthesis and the type of ZT phase led to the different photocatalytic activity. The $Zn_2Ti_3O_8$ phase was revealed to give better photocatalytic activity than the Zn_2TiO_4 phase and rutile TiO_2.

The kinetics of the photocatalytic degradation of phenol over ZT materials was investigated by using the first-order kinetic model as shown in Figure 6(b). The obtained plots were linear and have high correlation factors that were close to unity, indicating that the photocatalytic degradation of phenol over the ZT materials indeed followed the first-order reaction. The degradation rate constant on each ZT material could be determined from the slope of the plots, giving the values of 0.0353, 0.0355, and 0.0206 h^{-1} for the ZT-700, the ZT-900, and the ZT-1100, respectively. The ZT-700 and the ZT-900 gave a 1.7 times faster reaction rate as compared to the ZT-1100, again demonstrating the superior photocatalytic performance of the $Zn_2Ti_3O_8$ phase than the Zn_2TiO_4 phase and rutile TiO_2.

While the bandgap energy analysis of the ZT materials was used to reveal the active sites for phenol degradation, the characterization study using fluorescence spectroscopy could be used to understand the reason why the ZT-700 and ZT-900 gave similar activity but the ZT-1100 gave the lowest activity. As discussed previously, the ZT-1100 gave a higher emission intensity as compared to both ZT-700 and ZT-900 having nearly the same intensity levels. The higher emission intensity would be originated from the higher electron-hole recombination processes on the ZT-1100, which led to the lower photocatalytic activity. The presence of c-Zn_2TiO_4 phase and rutile TiO_2 could induce the high electron-recombination process on the ZT-1100. The rutile TiO_2 was reported to have a fast electron-hole recombination process [28], which seemed to cause the depletion of the photocatalytic activity in the ZT-1100. Based on the characterization and photocatalytic activity tests, it could be recommended here that the calcination temperature in the range of 700–900 °C is suitable to obtain the active $Zn_2Ti_3O_8$ phase in the ZT materials.

4. Conclusions

Effect of calcination temperatures (700, 900, 1100 °C) to prepare ZT materials by sol-gel method was studied by using zinc(II) nitrate and titanium(IV) isopropoxide as the precursor materials with the fixed mol ratio of 2:3. The FTIR, DR UV-vis, and fluorescence spectroscopies showed that the ZT-700 and the ZT-900 have similar properties, but the calcination temperature of 1100 °C resulted in the formation of different ZT phases. Based on the bandgap energy values, the ZT-700 and the ZT-900 would have the $Zn_2Ti_3O_8$ as the main phase, while the ZT-1100 would have Zn_2TiO_4 and rutile TiO_2. The photocatalytic degradation of phenol followed the first-order reaction with the degradation rate constants of 0.0353, 0.0355, and 0.0206 h^{-1} for ZT-700, ZT-900, and ZT-1100, respectively. The ZT materials having $Zn_2Ti_3O_8$ crystal phase exhibited higher photocatalytic activity than the one having Zn_2TiO_4 and rutile TiO_2 phases, which would be due to the lower electron-hole recombination on the ZT-700 and ZT-900 as compared to the ZT-1100. This study revealed that the calcination temperature of 700–900 °C shall be used to obtain the active $Zn_2Ti_3O_8$ phase.

Acknowledgements

This research was financially supported by the Directorate General of Strengthening Research and Development, Ministry of Research and Technology/National Research and Innovation Agency of Indonesia through the Higher Education Excellent Applied Research Grant (PTUPT 2020, No. 041/SP2H/AMD/LT/MULTI/L7/2020 and No. 002/MACHUNG/LPPM/SP2H-LIT-MULTI/AMD/VI/2020).

References

[1] Ratnawati, R., Enjarlis, E., Husnil, Y.A., Christwardana, M., Slamet, S. (2020). Degradation of phenol in pharmaceutical wastewater using TiO_2/pumice and O_3/active carbon. *Bull. Chem. React. Eng.* 15(1), 146–154, doi: 10.9767/bcrec.15.1.4432.146-154.

[2] Hayati, F., Isari, A.A., Fattahi, M., Anvaripour, B., Jorfi, S. (2018). Photocatalytic decontamination of phenol and petrochemical wastewater through ZnO/TiO_2 decorated on reduced graphene oxide nanocomposite: influential operating factors, mechanism, and electrical energy consumption. *RSC Advances*. 8(70), 40035–40053, doi: 10.1039/c8ra07936f.

[3] Jay, L., Chirwa, E.M.N. (2018) Pathway analysis of phenol degradation by UV/TiO_2 photocatalysis utilising the C-13 isotopic labelling technique. *Chem. Eng. Trans.* 70, 181–186, doi: 10.3303/CET1870031.

[4] Badli, N.A., Ali, R., Bakar, W.A.W.A., Yuliati, L. (2017). Role of heterojunction $ZrTiO_4$/$ZrTi_2O_6$/TiO_2 photocatalyst towards the degradation of paraquat dichloride and optimization study by Box–Behnken design. *Arab. J. Chem.* 10(7), 935–943, doi: 10.1016/j.arabjc.2016.02.011.

[5] Zhao, M., Bastakoti, B.P., Li, Y., Xu, H., Ye, J., Liu, Z., Yamauchi, Y. (2015). Mesoporous TiO_2/$Zn_2Ti_3O_8$ hybrid films synthesized by polymeric micelle assembly. *Chem. Commun.* 51(78), 14582–14585, doi: 10.1039/c5cc04903b.

[6] Sutanto, N., Saharudin, K.A., Sreekantan, S., Kumaravel, V., Akil, H.M. (2019). Heterojunction catalysts g-C_3N_4/-3ZnO-c-$Zn_2Ti_3O_8$ with highly enhanced visible-light-driven photocatalytic activity. *J. Sol-Gel Sci. Technol.* 93, 354–370, doi: 10.1007/s10971-019-05101-4.

[7] Chen, F., Yu, C., Wei, L., Fan, Q., Ma, F., Zeng, J., Ji, H. (2019). Fabrication and characterization of $ZnTiO_3$/$Zn_2Ti_3O_8$/ZnO ternary photocatalyst for synergetic removal of aqueous organic pollutants and Cr(VI) ions. *Sci. Total Environ.* 706, 136026, doi: 10.1016/j.scitotenv.2019.136026.

[8] Sahu, A., Chaurashiya, R., Hiremath, K., Dixit, A. (2018). Nanostructured zinc titanate wide band gap semiconductor as a photoelectrode material for quantum dot sensitized solar cells. *Sol. Energy*. 163, 338–346, doi: 10.1016/j.solener.2018.01.092.

[9] Platt, N.J., Kaye, K.M., Limburn, G.J., Cosham, S.D., Kulak, A.N., Palgrave, R.G., Hyetta, G. (2017). Order of magnitude increase in photocatalytic rate for hierarchically porous anatase thin films synthesized from zinc titanate coatings. *Dalton Trans.* 46(6), 1975–1985, doi: 10.1039/C6DT04431J.

[10] Yang, J., Swisher, J.H. (1996). The phase stability of $Zn_2Ti_3O_8$. *Mater. Charact.* 37(2–3), 153–159, doi: 10.1016/s1044-5803(96)00098-8.

[11] Budigi, L., Nasina, M.R., Shaik, K., Amaravadi, S. (2015). Structural and optical properties of zinc titanates synthesized by precipitation method. *J. Chem. Sci.* 127(3), 509–518, doi: 10.1007/s12039-015-0802-5.

[12] Arin, J., Thongtem, S., Phuruangrat, A., Thongtem, T. (2017). Template synthesis of Zn_2TiO_4 and $Zn_2Ti_3O_8$ nanorods by hydrothermal-calcination combined processes. *Mater. Lett.* 193, 270–273, doi: 10.1016/j.matlet.2017.01.142.

[13] Wang, L., Kang, H., Xue, D., Liu, C. (2009). Low-temperature synthesis of $ZnTiO_3$ nanopowders. *J. Cryst. Growth*. 311(3), 611–614, doi: 10.1016/j.jcrysgro.2008.09.071.

[14] Wang, C.L., Hwang, W.S., Chang, K.M., Ko, H.H., Hsi, C.S., Huang, H.H., Wang, M.C. (2011). Formation and Morphology of $Zn_2Ti_3O_8$ Powders Using Hydrothermal Process without Dispersant Agent or Mineralizer. *Int. J. Mol. Sci.* 12(2), 935–945, doi: 10.3390/ijms12020935.

[15] Chang, Y.S., Chang, Y.H., Chen, I.G., Chen, G.J., Chai, Y.L., Fang, T.H., Wu, S. (2004). Synthesis, formation and characterization of $ZnTiO_3$ ceramics. *Ceram. Int.* 30(8), 2183–2189, doi: 10.1016/j.ceramint.2004.01.002.

[16] Yu, C., Chen, F., Zhou, W., Xie, Y., Zeng, D., Liu, Z., Wei, L., Yang, K., Li, D., (2019). A facile phase transformation strategy for fabrication of novel Z-scheme ternary heterojunctions with efficient photocatalytic properties. *Nanoscale*. 11, 7720–7733, DOI: 10.1039/C9NR00709A.

[17] Mohammadi, M.R., Fray, D.J. (2010). Low temperature nanostructured zinc titanate by an aqueous particulate sol–gel route: Optimisation of heat treatment condition based on Zn:Ti molar ratio. *J. Eur. Ceram. Soc.* 30(4), 947–961, doi: 10.1016/j.jeurceramsoc.2009.09.031.

[18] Wang, J., Huang, J., Xie, H., Qu, A. (2014). Synthesis of g-C_3N_4/TiO_2 with enhanced photocatalytic activity for H_2 evolution by a simple method. *Int. J. Hydrog. Energy*. 39(12), 6354–6363, doi: 10.1016/j.ijhydene.2014.02.020.

[19] Musić, S., Popović, S., Maljković, M., Dragčević, Đ. (2002). Influence of synthesis procedure on the formation and properties of zinc oxide. *J. Alloys Compd.* 347(1–2), 324–332, doi: 10.1016/s0925-8388(02)00792-2.

[20] Liu, G., Li, G., Qiu, X., Li, L. (2009). Synthesis of ZnO/titanate nanocomposites with highly photocatalytic activity under visible light irradiation. *J. Alloys Compd.* 481(1–2), 492–497, doi: 10.1016/j.jallcom.2009.03.021.

[21] Eskandarloo, H., Badiei, A., Behnajady, M.A., Tavakoli, A., Ziarani, G.M. (2016). Ultrasonic-assisted synthesis of Ce doped cubic–hexagonal $ZnTiO_3$ with highly efficient sonocatalytic activity. *Ultrason. Sonochem.* 29, 258–269, doi: 10.1016/j.ultsonch.2015.10.004.

[22] Mrázek, J., Spanhel, L., Chadeyron, G., Matějec, V. (2010). Evolution and Eu^{3+} doping of sol-gel derived ternary $Zn_xTi_yO_z$ - nanocrystals. *J. Phys. Chem. C.* 114(7), 2843–2852, doi: 10.1021/jp9036217.

[23] Makuła, P., Pacia, M., Macyk, W. (2018). How to correctly determine the band gap energy of modified semiconductor photocatalysts based on UV-vis spectra. *J. Phys. Chem. Lett.* 9(23), 6814–6817, doi: 10.1021/acs.jpclett.8b02892.

[24] Conesa, J.C. (2013). Band structures and nitrogen doping effects in zinc titanate photocatalysts. *Catal. Today.* 208, 11–18, doi: 10.1016/j.cattod.2012.08.039.

[25] Mebrek, A., Alleg, S., Benayache, S., Benabdeslem, M. (2018). Preparation and characterization of spinel type Zn_2TiO_4 nanocomposite. *Ceram. Int.* 44(9), 10921–10928, doi: 10.1016/j.ceramint.2018.03.153.

[26] García-Ramírez, E., Mondragón-Chaparro, M., Zelaya-Angel, O. (2012). Band gap coupling in photocatalytic activity in ZnO–TiO_2 thin films. *Appl. Phys. A.* 108(2), 291–297, doi: 10.1007/s00339-012-6890-x.

[27] Zhu, T., Gao, S.-P. (2014). The stability, electronic structure, and optical property of TiO_2 polymorphs. *J. Phys. Chem. C.* 118(21), 11385–11396, doi: 10.1021/jp412462m.

[28] Li, B., Wu, S., Gao, X. (2020). Theoretical calculation of a TiO_2-based photocatalyst in the field of water splitting: A review. *Nanotechnol. Rev.* 9(1), 1080–1103, doi: 10.1515/ntrev-2020-0085.

Selected and Revised Papers from 3rd International Conference on Chemistry, Chemical Process and Engineering 2020 (IC3PE 2020) (https://chemistry.uii.ac.id/ic3pe/) (Universitas Islam Indonesia (UII), Labuan Bajo, Nusa Tenggara Timur, Indonesia by 30th September – 1st October 2020) after Peer-reviewed by Scientific Committee of IC3PE 2020 and Peer-Reviewers of Bulletin of Chemical Reaction Engineering & Catalysis. Editors: I. Istadi; Is Fatimah

BCREC2021_1

ORIGINALITY REPORT

17%	11%	12%	5%
SIMILARITY INDEX	INTERNET SOURCES	PUBLICATIONS	STUDENT PAPERS

PRIMARY SOURCES

1	Submitted to School of Business and Management ITB Student Paper	2%
2	link.springer.com Internet Source	1%
3	eprints.utm.my Internet Source	1%
4	academic-accelerator.com Internet Source	1%
5	iopscience.iop.org Internet Source	1%
6	Christyowati Primi Sagita, Leny Yuliati. "Photocatalytic degradation of phenol over carbon nitrides prepared by urea and melamine precursors", AIP Publishing, 2021 Publication	1%
7	www.mdpi.com Internet Source	1%
8	dokumen.pub Internet Source	1%

9	C P Sagita, L Yuliati. "Improved Visible Light Activity of Copper Oxide/Carbon Nitride Photocatalysts Prepared by Photodeposition for Phenol Degradation", IOP Conference Series: Materials Science and Engineering, 2021 Publication	1 %
10	repository.iti.ac.id Internet Source	1 %
11	Submitted to Program Pascasarjana Universitas Negeri Yogyakarta Student Paper	<1 %
12	Yehezkiel Steven Kurniawan, Kristine Anggraeni, Renny Indrawati, Leny Yuliati. "Selective betalain impregnation from red amaranth extract onto titanium dioxide nanoparticles", AIP Publishing, 2019 Publication	<1 %
13	Submitted to Universiti Teknologi Malaysia Student Paper	<1 %
14	res.mdpi.com Internet Source	<1 %
15	Hongbo Zhang, Jing Qiao, Guanshu Li, Siyi Li, Guowei Wang, Jun Wang, Youtao Song. "Preparation of Ce4+-doped BaZrO3 by hydrothermal method and application in dual-frequent sonocatalytic degradation of	<1 %

norfloxacin in aqueous solution", Ultrasonics Sonochemistry, 2018
Publication

16	Latifa Morjène, Fadhel Aloulou, Minoo Tasbihi, Michael Schwarze, Reinhard Schomäcker, Mongi Seffen. "New composite material based on Kaolinite, cement, TiO2 for efficient removal of phenol by photocatalysis", Environmental Science and Pollution Research, 2021 Publication	<1 %
17	Submitted to UT, Dallas Student Paper	<1 %
18	core.ac.uk Internet Source	<1 %
19	Guo, Xuyun, Weiqiang Lv, and Xiao-Yuan Li. "Additive-Free Shape-Invariant Nano-to-Micron Size- Tuning of Cu2O Cubic Crystals by Square-Wave Voltammetry", The Journal of Physical Chemistry C Publication	<1 %
20	Lili Lu, Rui Shan, Yueyue Shi, Shuxiao Wang, Haoran Yuan. "A novel TiO2/biochar composite catalysts for photocatalytic degradation of methyl orange", Chemosphere, 2019 Publication	<1 %

21	www.hadinur.com Internet Source	<1%
22	www.osha.gov Internet Source	<1%
23	Ismail, A.A.. "Mesostructure Au/TiO"2 nanocomposites for highly efficient catalytic reduction of p-nitrophenol", Journal of Molecular Catalysis. A, Chemical, 201206 Publication	<1%
24	Ivonne Linares-Hernández, Luis Antonio Castillo-Suárez, Jorge G. Ibanez, Ruben Vasquez-Medrano et al. "Degradation of commercial paraquat in a solar-Fenton pilot lagoon using iron oxalate as a chelating agent: Hydro-thermal analysis with CFD", Journal of Photochemistry and Photobiology A: Chemistry, 2022 Publication	<1%
25	Divya Gupta, Rohit Chauhan, Navneet Kumar, Vikash Singh, Vimal Chandra Srivastava, Paritosh Mohanty, Tapas Kumar Mandal. "Enhancing photocatalytic degradation of quinoline by ZnO:TiO2 mixed oxide: Optimization of operating parameters and mechanistic study", Journal of Environmental Management, 2020 Publication	<1%

26	M. P. Belciug, A. M. Modro, T. A. Modro, E. R. Rohwer, A. Zwierzak. "PHOSPHONIC SYSTEMS. 6. DIETHYL 2-METHYLPENTENYLPHOSPHONATES AS A MODEL FOR STUDIES OF THE STABILITY OF UNSATURATED PHOSPHONIC ESTERS", Phosphorus, Sulfur, and Silicon and the Related Elements, 1991 Publication	<1 %
27	Pattarasuda Naknam. "Au/ZnO and Au/ZnO−Fe_2O_3 Prepared by Deposition−Precipitation and Their Activity in the Preferential Oxidation of CO", Energy & Fuels, 10/15/2009 Publication	<1 %
28	Tamao Ishida, Toru Murayama, Ayako Taketoshi, Masatake Haruta. "Importance of Size and Contact Structure of Gold Nanoparticles for the Genesis of Unique Catalytic Processes", Chemical Reviews, 2019 Publication	<1 %
29	Xiaobo Chen, Samuel S. Mao. "Titanium Dioxide Nanomaterials: Synthesis, Properties, Modifications, and Applications", Chemical Reviews, 2007 Publication	<1 %
30	Xin-Yuan Xie, Li-Yun Li, Pei Zhan, Ming Liang, Shu-Ming Xie, Jian-Xin Meng, Yan Bai, Wen-Jie	<1 %

Zheng. "Fast one-step synthesis of ZnO sub-microspheres in PEG200", Journal of Materials Science, 2013
Publication

31	docplayer.com.br Internet Source	<1 %
32	dspace.vutbr.cz Internet Source	<1 %
33	ir.cftri.res.in Internet Source	<1 %
34	mdpi-res.com Internet Source	<1 %
35	"Photocatalysts in Advanced Oxidation Processes for Wastewater Treatment", Wiley, 2020 Publication	<1 %
36	LOKESH BUDIGI, MADHUSUDHANA RAO NASINA, KALEEMULLA SHAIK, SIVAKUMAR AMARAVADI. "Structural and optical properties of zinc titanates synthesized by precipitation method", Journal of Chemical Sciences, 2015 Publication	<1 %
37	Jan Mrázek, Lubomir Spanhel, Geneviève Chadeyron, Vlastimil Matějec. " Evolution and Eu Doping of Sol–Gel Derived Ternary Zn Ti O	<1 %

- Nanocrystals ", The Journal of Physical Chemistry C, 2010

Publication

Exclude quotes	Off	Exclude matches	Off
Exclude bibliography	On		

BCREC2021_1

GRADEMARK REPORT

FINAL GRADE

/0

GENERAL COMMENTS

Instructor

PAGE 1

PAGE 2

PAGE 3

PAGE 4

PAGE 5

PAGE 6

PAGE 7

PAGE 8

PAGE 9